



## Full Text View

[Volume 28, Issue 10 \(October 1998\)](#)

### Journal of Physical Oceanography

 Article: pp. 1999–2018 | [Abstract](#) | [PDF \(440K\)](#)

# The Impact of Southern Ocean Sea Ice in a Global Ocean Model

**Achim Stössel and Seong-Joong Kim**

*Department of Oceanography/Texas Center for Climate Studies, Texas A&M University, College Station, Texas*

**Sybren S. Drijfhout**

*Royal Netherlands Meteorological Institute, De Bilt, the Netherlands*

(Manuscript received February 12, 1997, in final form December 19, 1997)

DOI: 10.1175/1520-0485(1998)028<1999:TIOSOS>2.0.CO;2

### ABSTRACT

Most of the Southern Ocean (SO) is marginally stably stratified and thus prone to enhanced convection and possibly bottom-water formation whenever the upper ocean is cooled or made more saline by ice formation. Sea ice modifies the heat and freshwater fluxes, which in turn constitute a critical surface condition in this sensitive region of intense vertical exchange. The authors investigate the effect of SO sea ice in modifying these fluxes in a global, coarse-resolution, primitive-equation ocean general circulation model, which has been coupled to a comprehensive dynamic–thermodynamic sea ice model. Specifically, the long-term impact of a series of modifications in the formulation of the sea ice model and its forcing on quantities such as the overturning circulation, the deep ocean water-mass characteristics, the sea ice thickness, the strength of convection, as well as the strength of the major volume transports are investigated. The results indicate that the rate of Antarctic bottom-water formation is strongly coupled to the local sea ice processes in the SO, which in turn vary sensitively depending on their model formulation and their forcing from the atmosphere. The largest impacts arise from the effect of brine release due to sea ice formation and that of employing more variable winds over SO sea ice.

### 1. Introduction

A main component driving global climate is the ocean. Both the atmospheric and oceanic circulation determine the air–sea heat exchange, which acts to moderate the equator-to-pole temperature difference. In general, a large heat flux from the ocean

#### Table of Contents:

- [Introduction](#)
- [Model description](#)
- [Reference simulation](#)
- [Sensitivity experiments](#)
- [Results and discussions](#)
- [Summary and conclusions](#)
- [REFERENCES](#)
- [TABLES](#)
- [FIGURES](#)

#### Options:

- [Create Reference](#)
- [Email this Article](#)
- [Add to MyArchive](#)
- [Search AMS Glossary](#)

#### Search CrossRef for:

- [Articles Citing This Article](#)

#### Search Google Scholar for:

- [Achim Stössel](#)
- [Seong-Joong Kim](#)
- [Sybren S. Drijfhout](#)

to the atmosphere is associated with strong vertical motion in the ocean. The most vigorous vertical motions of the world's oceans thus occur in high latitudes, where dense water is produced at the ocean's surface by cooling to the freezing point, and beyond that, by brine release through sea ice formation. Sea ice modifies the heat exchange and freshwater budget at the ocean's surface. Specifically, sea ice may locally inhibit deep convection through melting and enhance it elsewhere through freezing. The latter may eventually modify the rates of deep- and bottom-water formation, which themselves determine the global deep ocean water-mass properties and influence the global thermohaline circulation.

While in the Northern Hemisphere sea ice mainly acts to reduce convection due to sea ice melt at the convective sites (e.g., [Häkkinen 1995](#)), convection in the mostly marginally stably stratified regions around Antarctica is often enhanced by the addition of brine associated with freezing (e.g., [Martinson 1990](#); [Gordon and Huber 1990](#)). As pointed out in several regional observational and modeling studies in the Southern Ocean (SO) ([Schlosser et al. 1990](#); [Gordon 1978](#); [Jacobs and Comiso 1989](#); [Martinson et al. 1981](#); [Killworth 1983](#); [Foster and Carmack 1976](#); [Gill 1973](#); [Akitomo et al. 1995](#); [McPhee 1995](#); [Worby et al. 1996](#); [Oshima et al. 1996](#)), as well as in global coupled atmosphere–ocean general circulation model (A–OGCM) studies ([Manabe et al. 1992](#); [Murphy and Mitchell 1995](#); [Washington and Meehl 1996](#); [Weatherly et al. 1997](#); [Cubasch et al. 1994](#); [Gordon and O'Farrell 1997](#)), a subtle balance exists between the comparatively thin and mobile sea ice cover, the rate of local convection, and the rate of Antarctic Bottom Water (AABW) formation. Brine rejection destabilizes the stratification of the typical SO water column, ultimately inducing deep convection; simultaneously, however, heat from deeper water masses is brought to the surface inducing sea ice melt ([Martinson 1990](#)). Since we are dealing with a sensitive region of enhanced communication between the surface and the deep ocean, the question arises: how sensitively do the global deep-ocean water-mass properties depend on the SO surface conditions?

[Maier-Reimer \(1993\)](#) investigated the direct impact of brine release on the rate of deep convection and bottom-water formation with the global large-scale geostrophic (LSG) OGCM ([Maier-Reimer et al. 1993](#); [Mikolajewicz and Maier-Reimer 1990](#); [Hasselmann 1982](#)) and found that the deep water is substantially cooled by brine release. [Goosse et al. \(1997\)](#) also found a reduction in the deep ocean's temperature of their primitive-equation global OGCM whenever the brine-release effect of sea ice was considered. This suggests that freezing and melting of sea ice has a direct impact on the deep-water properties.

In OGCMs, the rate of AABW formation also seems to have a strong impact on the strength of the Antarctic Circumpolar Current (ACC). Using a version of the Modular Ocean Model (MOM) ([Bryan 1969](#); [Cox 1984](#); [Semtner 1976](#); [Pacanowski 1995](#)), [Cai and Baines \(1996\)](#) found that in the presence of a topographic ridge across Drake Passage, AABW produced in the Weddell Sea provides a major contribution in driving the ACC. The results of [Drijfhout et al. \(1996, hereafter DHLM\)](#) using the Hamburg Ocean Primitive Equation (HOPE) Model ([Wolff et al. 1997](#); [Legutke et al. 1997](#); [Latif et al. 1994](#)) support this finding.

Several attempts have been made to mimic the effect of sea ice in global OGCMs that do not include a sea ice model. By increasing the sea surface salinity artificially up to 35.0 psu south of 70°S in the three winter months, [England \(1992, 1993\)](#), using a version of the MOM OGCM, obtained a substantially increased overturning cell adjacent to Antarctica and an enhanced intrusion of AABW across the equator, associated with more realistic deep ocean thermohaline properties. In a similar MOM OGCM version, [Toggweiler and Samuels \(1995\)](#) restored the surface salinity to more realistic values over the Weddell and Ross Seas and concluded that the brine-release effect should be weaker than the “salinity enhancement” proposed by [England \(1993\)](#) and that biases in the model's deep ocean salinities are due to other deficiencies such as an insufficient representation of the Circumpolar Deep Water (CDW).

The general intention of our study is to improve the high-latitude processes in the framework of an ocean climate model and to understand the influence of sea ice on the large-scale hydrographic properties and the long-term thermohaline conveyor-belt circulation. In the present study, we investigate the impact of SO sea ice on the convection rate, the rate of AABW formation, the strength of the ACC mass transport, the Southern Hemisphere overturning cell associated with the intrusion of AABW across the equator, and the thermohaline properties of the deep ocean. This study is an extension and further development of preliminary studies ([Stössel 1996, 1997](#)). In those studies, using the HOPE OGCM including sophisticated sea ice dynamics but a simple formulation of sea ice thermodynamics (essentially using the version of DHLM), the impact of brine release, of salinity enhancement, and of new-ice growth in the ice-free part of a model grid cell were investigated. All three experiments revealed significant changes in the SO convection rate, the meridional overturning circulation, and the deep ocean temperature and salinity. The ice cover also changed substantially, primarily due to changes in the ocean's response.

This paper presents a more thorough investigation involving a series of other modifications in the description of SO sea ice including its forcing from the atmosphere. Additionally, the sea ice thermodynamics have been replaced by a more comprehensive formulation allowing for a more realistic representation of the surface fluxes over the sea ice–ocean admixture.

In the following section, the model and its present configuration will be described. [Section 3](#) shows some basic results of

the reference version of the present model. [Section 4](#) describes the experiments and their motivation. [Section 5](#) shows the main results of the sensitivity experiments focusing on selected quantities in the subsections. In [section 6](#), the results are summarized, discussing the relevant findings and drawing some conclusions.

## 2. Model description

The tool for this investigation is a version of the HOPE sea ice–ocean GCM (see previous section). In comparison to the more commonly used MOM model, the HOPE model employs a prognostic free surface, has a more detailed representation of the bottom topography (variable layer thickness at the bottom), and employs sea ice dynamics using the viscous–plastic constitutive law of [Hibler \(1979\)](#) to describe the internal ice stress. It is horizontally discretized on an Arakawa E grid and uses partly implicit methods to solve the momentum equations.

In comparison to the standard LSG model, the HOPE model contains nonlinear momentum advection and differs the same way with respect to sea ice dynamics as compared with the MOM model (see above). Due to the usage of the full primitive equations, the HOPE model operates with a considerably shorter time step than the LSG model. A centered differencing scheme is employed for tracer advection (thus using explicit horizontal and vertical diffusivities) as opposed to an upwind scheme in the LSG model.

Our starting point is the coarse-resolution ( $3.5^\circ \times 3.5^\circ \times 11$ -layer) HOPE version of DHLM. With this global sea ice–ocean model we can afford a series of sensitivity experiments toward near-equilibrium solution. We note that this cannot be readily achieved with high-resolution (e.g., eddy resolving) OGCMs nor with coupled A–OGCMs.

The difference to DHLM is composed of two major modifications: The first consists of a tuning of the model to achieve a more realistic strength of the ACC, which was severely underestimated in the DHLM version. The new equilibrium integration (several thousand years) is based on a larger vertical diffusion ( $0.8 \times 10^{-4} \text{ m}^2 \text{ s}^{-1}$  instead of  $0.5 \times 10^{-4} \text{ m}^2 \text{ s}^{-1}$ ) and a lower horizontal viscosity (maximum at the equator:  $2 \times 10^5 \text{ m}^2 \text{ s}^{-1}$  instead of  $3 \times 10^5 \text{ m}^2 \text{ s}^{-1}$ ), as well as higher restoring values for the wintertime sea surface salinity in the ice-free part of model grid cells south of  $70^\circ\text{S}$  (35.0 psu, following [England 1992](#)). Otherwise, the upper-layer (50 m thick) salinity is no longer restored to the surface salinity of [Levitus \(1982\)](#) but rather to the vertically averaged salinity for the upper 50 m of that dataset. No salinity restoring is used under sea ice, and the momentum flux under sea ice is provided by the ice–ocean stress. Furthermore, whenever there is sea ice in a model grid cell, the upper-layer temperature is assumed to be at the freezing point. The comprehensive heat-budget calculation is only used in grid cells where there is ice initially, mainly in order not to alter the global temperature forcing of the model. These conditions are assumed to be most realistic in the framework of this ocean climate model.

All other forcing conditions are identical to DHLM, that is, climatological monthly mean fields for the wind forcing ([Hellerman and Rosenstein 1983](#)) and the sea surface temperature restoring (COADS; [Woodruff et al. 1987](#)), as well as the restoring timescales for surface temperature (80 days) and salinity (40 days).

The second part of the modifications are essentially based on findings described in [Stössel et al. \(1996\)](#), who concluded that the original (ad hoc) description of the thermodynamic part of the HOPE sea-ice model responded too sensitively to the atmospheric forcing. We thus replaced the sea ice thermodynamics to determine the ice growth rate through a comprehensive surface heat-balance calculation for the ice-free and ice-covered part of a model grid cell with options, among others, to include a prognostic snow cover. Details about this formulation are found in [Owens and Lemke \(1990\)](#) and [Stössel and Owens \(1992\)](#), and about its implementation into the HOPE model in [Stössel et al. \(1996\)](#), [Legutke et al. \(1997\)](#) and [Wolff et al. \(1997\)](#). This modification constitutes the essential upgrade to the HOPE version used in [Stössel \(1997\)](#).

## 3. Reference simulation

After introducing the modifications described in the previous section, we integrated the model to a near-equilibrium state, the results of which we use as the reference case for the sensitivity investigations. This reference integration was initiated from a 10 000-year equilibrium integration. Some basic results of the reference integration are illustrated in the following and compared to the results of DHLM and to observations, thereby focusing specifically on the high southern latitude performance.

[Figure 1](#) shows the global meridional overturning. The overall structure of sinking water masses in the northern and southern high latitudes is clearly visible. The Northern Hemisphere overturning cell, which is entirely associated with the formation of North Atlantic Deep Water (NADW) is substantially stronger than what has been produced by DHLM ( $30 \text{ Sv}$ ;  $\text{Sv} \equiv 10^6 \text{ m}^3 \text{ s}^{-1}$ ) and derived from observations ([Macdonald and Wunsch 1996](#): 27 Sv).

The decisive gauge for the conveyor-belt circulation, however, is the NADW outflow at  $30^\circ\text{S}$ . The model yields 18 Sv for this quantity, which is similar to DHLM and in very good agreement with [MacDonald and Wunsch \(1996\)](#) as well as

Schmitz (1996). The strength of the SO overturning cell—often associated with AABW formation (Cai and Baines 1996) or AABW overturning (England 1993)—is almost identical to DHLM, whereas the overall Southern Hemisphere (SH) cell (associated with the intrusion of AABW across the equator)—termed “SH bottom-water cell” in England (1993) and “southern sinking cell” in Cai and Baines (1996)—has, in comparison to DHLM, strengthened from 4 to more than 12 Sv. This figure is also supported by the calculations of MacDonald and Wunsch, though the error bars are large for this particular quantity. The overturning cells of the Atlantic and the Pacific (not shown) are similar to DHLM, except for the differences already noticed from the global meridional overturning.

Other key quantities are 95 Sv for the Drake Passage throughflow, 20 Sv for the Indonesian Throughflow, and 0.8 PW for the northward heat transport across  $\Phi = 30^\circ\text{N}$  in the Atlantic. While the latter two values lie within the observed uncertainty range, the ACC strength is still underestimated by 30–40 Sv (Whitworth and Peterson 1985; MacDonald and Wunsch 1996). All three values, together with the NADW outflow, are in the range of the model variability of DHLM. The changes are consistent with an overall higher diffusion rate and enhanced ice formation around Antarctica. The Arctic ice volume is  $21\,000\text{ km}^3$ , and the Antarctic ice volume  $3500\text{ km}^3$ , compared to estimated observed annual means of  $\approx 30\,000\text{ km}^3$  and  $\approx 10\,000\text{ km}^3$ , respectively (Weatherly et al. 1997).

Figure 2 shows observed (left) and modeled (right) potential temperature (top) and salinity (bottom) sections along the western Atlantic (averaged between  $10^\circ$  and  $60^\circ\text{W}$ ). The  $0^\circ\text{C}$  isotherm in the SH is shifted farther north compared to the observation and also compared to DHLM, commensurate with a stronger intrusion of AABW. As a result, the water below 2000 m is cooler and more stratified than observed. The stronger intrusion of AABW is also seen in the salinity section. The core of the NADW as well as the Antarctic Intermediate Water (AAIW) can be well identified, though the appearance of the latter is more diffuse than observed.

Figure 3 shows the modeled annual-mean potential energy release associated with convective overturning. The convectively active regions are mostly confined to the Greenland–Iceland–Norwegian (GIN) sea and the Labrador Sea in the Northern Hemisphere (NH), as well as the Weddell, Ross, and Amundsen Seas in the SH, fairly consistent with the observed locations of NADW and AABW formation (see section 1). This result is similar to what Maier-Reimer et al. (1993) achieved with the LSG model, using essentially the same forcing and boundary conditions. The seasonal cycle of a hemispherical average of this quantity is represented by full lines in Fig. 5.

The winter ice thickness patterns are given in Fig. 4. As is obvious from Fig. 4 (left), the resolution of this model is too coarse to reproduce a reasonable ice thickness distribution in the Arctic Ocean. Thus, ice tends to pile up northwest of Greenland, since this extends up to the North Pole in the model. Another region of excessive ice thickness is visible in the east Siberian Sea, which is mostly due to the poor wind stress climatology. The latter is also critical for driving SO sea ice (Stössel et al. 1990). This explains some of the discrepancies in its reproduction in our model (Fig. 4, right). The regional underestimation of sea ice thickness, however, is mostly due to excessive convective overturning, leading to warmer water (CDW) being continuously entrained into the mixed layer. We thus deal with widespread situations of vigorous open ocean convection (e.g., Carmack 1990) associated with an extensive upward oceanic heat flux (Legutke et al. 1997). An indication of the excessive vertical mixing is given in Fig. 15 in terms of temperature and salinity profiles from the central Weddell Sea.

#### 4. Sensitivity experiments

Our intention is to identify the most crucial constituents of sea ice that could play an important role in global ocean modeling. These constituents can be separated between those that are related to the physical description of sea ice and those that originate from the particular forcing of the sea ice–ocean admixture from the atmosphere. Both refer to processes related to a more realistic treatment of sea ice in a vertically highly active, and thus sensitive, region of the World Ocean.

The sensitivity experiments are structured in four themes (Table 1). The first addresses the effect of sea ice in modifying the sea surface salinity through brine release during sea ice formation (and freshwater release during sea ice melt) (see section 1). Our first experiment investigates the effect of its neglect (expt SSI). A commonly used substitute for this first-order sea ice effect in the SO is that of wintertime “salinity enhancement” (see section 1). In order to compare the impact of this (unphysical) measure relative to including a “real,” interactive sea ice component, we replace the interactive brine- (and freshwater) release effect by employing salinity restoring under sea ice including wintertime salinity enhancement in otherwise the same model environment (expt SSI.WSE). We follow England (1992) and employ a surface salinity of 35.0 psu in the two southernmost grid rows from July through September. The motivation for this experiment is to investigate the effect of this substitution. We note that the specific figure used here is fairly high and has been criticized by Toggweiler and Samuels (1995) (see section 1).

The second set of experiments deals with changes in the thermodynamic treatment of sea ice. As referred to in section 1, the way new-ice formation in the ice-free part of a model grid cell is formulated is expected to have some impact on the rate of AABW formation. In the first experiment, we investigate this and neglect that part of new-ice growth that contributes to



ice thickness growth (expt NTP), while we do not neglect the part that contributes to lead closing (i.e., increase of ice compactness). The other experiment under this theme addresses the role of a snow cover on sea ice (expt SNC). Snow has two major effects on the seasonal representation of sea ice: 1) Its insulation effect (roughly 1/7 of the thermal conductivity of ice), which leads to substantially lower ice growth rates, and 2) its albedo effect (the albedo of new snow is about 15% higher than that of snow-free sea ice), which delays surface ice melt resulting from insolation. While both effects yield an opposite effect on sea ice growth, the former one dominates in SO sea ice. Instead of employing the prognostic snow formulation, we specify a 10-cm snow cover whenever the mean ice thickness is greater than 10 cm. The imposed snow cover is only used to account for its effect on the thermal insulation and modified albedo. The snow mass is subtracted after the heat budget calculations and is thus not advected and has no impact on the freshwater balance. This was done in order to isolate the pure thermodynamic effect of snow-covered sea ice. The snow albedo itself is allowed to vary in response to the surface temperature (i.e., 0.85 if the diagnosed snow surface temperature is below freezing and 0.75 otherwise; see [Stössel and Owens 1992](#)).

In the third set of experiments, we investigate the role of ice dynamics, again in terms of common simplifications made in ocean models that include a sea ice component (e.g. [Murphy 1995](#); [Meehl and Washington 1990](#); [Cubasch et al. 1992](#); [Manabe et al. 1992](#)). In the first case, we neglect ice dynamics altogether (expt NID), that is, we treat the sea ice component as being purely thermodynamic. This would be the simplest implementation of a sea ice component in an OGCM. A step toward including effects of sea ice dynamics in global ocean models is to allow sea ice to be advected with the surface (upper layer) ocean currents while assuming free-ice drift below a specified cutoff thickness (e.g., [Manabe et al. 1992](#)) or employing a simple viscous rheology (e.g., [Maier-Reimer et al. 1993](#)) in order to prevent excessive ridging (dynamic ice accumulation) in convergent drift regions. We thus investigate the effect of dynamically forcing sea ice from underneath, that is, indirectly by the upper-layer ocean model currents (expt DFC) instead of forcing it directly from above by the winds. Note that in this experiment the ice-covered ocean is wind-driven in the same way as the ice-free ocean, commensurate, for example, with [Hibler and Bryan \(1987\)](#), [Manabe et al. \(1992\)](#), and [Cubasch et al. \(1994\)](#). The dynamic sea ice formulation is unchanged from the reference case.

The final set of experiments deals with the aspect of a more realistic forcing of sea ice from the atmosphere. As pointed out in earlier research (for the Arctic Ocean: e.g., [Hibler and Bryan 1987](#); [Hibler and Walsh 1982](#); [Legutke 1992](#); for the Southern Ocean: e.g., [Stössel et al. 1990](#); [Wu et al. 1996](#); [Stössel 1996](#)), the most sensitive atmospheric forcing field for pack ice is the wind field. Its effect on sea ice is threefold: 1) the overall pattern of the time-mean fields has to match the prevailing pressure systems in order to avoid unrealistic accumulation or divergence of the sea ice pack; 2) due to the nonlinear interactions between ice dynamics and thermodynamics, synoptic-scale variability in the wind forcing plays an important role in sea ice simulations, especially new-ice growth in leads and polynyas; and 3) the turbulent heat fluxes are increased with a higher variability in the wind forcing, leading to enhanced thermodynamic ice growth and melt. We investigate the impact of just modifying the wind forcing over SO sea ice. First, we run an experiment superimposing daily wind fluctuations derived from the European Centre for Medium-Range Weather Forecasts (ECMWF) analyses on to the climatological monthly means of [Hellerman and Rosenstein \(1983\)](#) (expt DWF). To eliminate the dynamic and the thermodynamic effect of applying higher variability, we apply the daily fluctuations to the dynamic forcing only (expt DWF.DFO), while the monthly mean wind speed is used to calculate the turbulent heat fluxes. In order to consolidate the effect of the latter, we conduct an additional experiment (expt ETH), where we employ the monthly winds for both the dynamic and the thermodynamic sea ice forcing but increase the wind speed for the heat flux calculation effectively by a factor of 3, thus roughly corresponding to typical increases in wind speed observed with a change from monthly mean to daily variability. This modification is introduced over the sea ice regions of both hemispheres.

## 5. Results and discussions

In this section, the results of the sensitivity experiments will be discussed. Depending on the severity of the impact of any of the changes referred to in the previous section, the model integration time has been varied from 300 up to 1200 years ([Table 1](#)). This leads to a near-equilibrium state following the criteria of [England \(1993\)](#), that is, with a remaining climate drift in global-mean temperature and salinity at all model layers of less than 0.01°C and 0.001 psu per century. This is associated with a negligible drift in the strength of the ACC. It is noted that these criteria are somewhat arbitrary and that a proper equilibrium state for the abyssal ocean will not be reached until about 4000 years of integration (e.g., [Danabasoglu et al. 1996](#)). The asymptotic approaches toward the actual equilibrium solutions, however, suggest that we reached this solution within about 5% in all experiments. Since we do not expect significant changes to occur by capturing the remaining 5%, another 3000 years of integration per experiment does not seem to be justified. The initial condition for all experiments are those of the reference simulation shown in [section 3](#).

We will discuss the results by analyzing distinct quantities at a time. First, we will investigate the rate of convection. We will then turn to the strength of the global meridional overturning and try to relate this to the rate of bottom- and deep-water formation. A further gauge of the latter is a change in the deep ocean's temperature and salinity. Finally, we investigate the associated changes in sea ice, specifically its thickness pattern, together with some related hydrographic features around Antarctica.

## a. Convection

We monitor the strength of convection by computing the associated potential energy release. The areal distribution of the annual-mean potential energy release of the reference simulation was given in [Fig. 3](#). The seasonal variation of both NH and SH convection is represented in [Fig. 5](#) as a hemispheric average beyond the latitudes of 40°. The full lines on all graphs represent the reference simulation (REF). A strong seasonal cycle is registered in both hemispheres with the NH maximum in February and the SH maximum in August.

While the NH is hardly affected, strong differences occur in the SH between REF and experiments SSI and SSI.WSE ([Fig. 5a](#)). In the SSI case, SH convection is substantially lower from June through September. This is expected since the neglect of brine release is primarily associated with a stabilization of the water column. Enhanced convection is seen in SH spring (October–November), due to the opposite effect that ice melt in this experiment is not associated with freshwater release. According to these results, convection is mostly determined by cooling. Nevertheless, the brine-release effect during SO sea ice formation can account for as much as 50% of the total (hemispherically averaged) convective potential energy release.

The SSI.WSE experiment shows the opposite behavior. The convection in the SH experiences a substantial increase during and shortly after the months of introduced salinity enhancement (July–September). It also shows that the salinity enhancement induces more convection than the “real” sea ice effect. This can be attributed to a missing feedback: With an interactive sea ice component, enhanced open ocean convection would lead to instantaneous ice melt, thus reducing brine release and eventually reducing convection as well. With the salinity-enhancement substitution, on the other hand, the sea surface salinity is relaxed to higher salinities inducing higher convection, regardless of the instantaneous vertical ocean heat flux and sea ice conditions.

Experiments NTP and SNC yield a slight reduction in convection ([Fig. 5b](#)). Experiment NTP mainly leads to a decrease in convection during the SH ice growth season from June to August. The way new-ice thickness growth is formulated thus has some impact on the convection rate, though by far not as large as we saw in the SSI experiments. A similar experiment with the more original DHLM model version using simplified sea ice thermodynamics (see [section 1](#)) revealed a much stronger effect. This occurred because of the simpler and much more sensitive surface heat-flux calculation in that model, leading to substantially higher new-ice growth rates and thus AABW formation after introducing explicit new-ice thickness growth. This difference in the sensitivity underlines the importance of a careful determination of the surface fluxes in subgrid-scale openings within the ice pack of an ocean climate model. Accounting for the effect of snow (SNC) reduces convection in SH fall and winter. This feature is consistent with the effect of enhanced insulation from the cold atmosphere, which leads to warmer ice surface temperatures and thus lower ice growth rates in fall and winter (see previous section).

The next two experiments (NID and DFC) yield a stronger decrease in SH winter convection ([Fig. 5c](#)). In the case of NID, this feature is consistent with the fact that there is no mechanism allowing the ice pack to diverge. This inhibits the creation of dynamically induced leads or polynyas, which are normally the sites of most intense cooling and sea ice growth leading to brine release (see previous section). Convection in the DFC case being similar to the NID case implies that the commonly used assumption of forcing the ice dynamically with the upper-ocean currents only, and thereby neglecting the direct wind forcing, has a nonnegligible impact on SH wintertime convection.

Finally, the impact of higher wind variability ([Fig. 5d](#)) shows an increase throughout the convectively active seasons in SH fall in the DWF case. This is expected since the higher wind variability has both the effect of enhancing the turbulent heat flux, and thus the overall ice growth rate, and of enhancing the lead fraction, which provides an additional source for new-ice growth. The DWF.DFO case, however, yields hardly any change versus REF. Thus, the pure situation of more frequent formation of leads associated with the higher wind variability does not seem to enhance convection, unless it is combined with enhanced turbulent heat fluxes due to the associated higher wind speeds. This result is manifested in the ETH experiment, where the difference of SH convection to REF is quite similar to the difference between experiments DWF and DWF.DFO.

Except for DWF and DWF.DFO, all changes in the model description of sea ice were introduced in both hemispheres. Nevertheless, NH convection is hardly influenced, implying that our sea ice description does not seem to seriously modify convection in the GIN and Labrador Seas. While this appears consistent with earlier findings, we have to keep in mind that our NH results are not very meaningful due to the poor resolution of the Arctic Ocean, especially with respect to the export of sea ice through Fram Strait (see [section 1](#)).

## b. Meridional overturning

The meridional overturning is an integrated quantity, which would indicate large-scale changes in the circulation. [Figure 1](#) shows the situation for the reference integration as discussed in [section 3](#).

The SSI experiment (Fig. 6, top) shows a slight reduction of the SH overturning cell associated with the amount of AABW penetrating into the tropical ocean. Simultaneously, we find an increase and shallowing of the SO overturning cell. The tendency of this result is consistent with what was found in Stössel (1997) (see section 1), except that the effect on the SH cell is weaker.

The enhancement of the SO cell, which is composed of a zonal integration south of 70°S, seems to be associated with a shift of the convective activity from “lower latitude” (north of 70°S) to “higher latitude” (south of 70°S) regions around Antarctica. Figure 7 (top) shows the horizontal pattern of the difference in potential energy release related to wintertime convection of SSI minus REF. An enhancement of convection in the south-central Weddell Sea and the western Ross Sea is obvious. Dividing the SO cell into the contributions of the individual higher-latitude embayments, we find that the increase of the SO cell is mainly due to the increase in the Weddell Sea overturning. This is a result of an intense background convection already present in the REF case. In this region, the annual net freezing rate is predominantly negative. There, ice melt thus leads to additional salt input in the SSI case followed by an enhancement of convection.

The SH cell reflects changes in the total amount of AABW penetrating into the world’s oceans. AABW is a product of water masses formed in high-latitude embayments, flowing down into the deep ocean basin of the SO, where it becomes subject to entrainment of overlying (deep) water (Price and Baringer 1994, and references therein). (One could be tempted to associate the water formed in the model’s high-latitude embayments with Weddell or Ross Sea Bottom Water, but since the continental shelves in this model version are poorly resolved, we will refrain from doing so.) In the model, the overlying water is modified by open ocean convection. In the SSI case, the rate of lower-latitude open ocean convection decreases as the surface water becomes fresher. This seems to be roughly compensated by the increased outflow from the Weddell Sea resulting from the release of brine during melting (see next section).

Goosse et al. (1997) and Maier-Reimer (1993) encountered a decrease of the SH cell of up to 10 Sv in corresponding salty sea ice experiments with their models (see section 1). A common difference in their SO surface conditions compared to ours is a full salinity relaxation toward the Levitus (1982) climatology everywhere, that is, also under sea ice. Without salinity enhancement, as in the case of Goosse et al. (1997) and Maier-Reimer (1993), full salinity relaxation counteracts the real sea ice effect in wintertime because the climatology dictates surface water that is too fresh (see section 4). As the background convection is weaker, a superimposed neglect of brine release may enhance the sensitivity with respect to a change in the SH overturning to eventually shut it down almost entirely.

The SSI.WSE experiment (Fig. 6, bottom) shows a similar impact on the strength of the SO overturning as the SSI case. The vertical extension of the SO cell is larger than in the SSI case, indicating deeper convection. This is mostly due to enhanced convection in the eastern Ross Sea and the Amundsen Sea south of 70°S (Fig. 7, bottom). This figure also reveals a substantial increase in lower-latitude convection. Both features are commensurate with an increase in total SH convection (Fig. 5a). Overall, this leads to enhanced AABW formation, the global impact of which is indicated in an enhanced SH cell versus SSI.

In the NTP and the SNC experiments, the impact on the meridional overturning cells is negligible, except for a slight increase of the SO cell in NTP (not shown). This weak impact is consistent with the relative weak impact on SH convection (Fig. 5b).

A strengthening of 2 Sv in the SO overturning is found in the NID and DFC experiments, though only during the winter months (not shown). The respective SH cells remained nearly unchanged in spite of the fairly substantial decrease in SH convection (Fig. 5c). These changes follow the same reasoning as in the SSI case (Fig. 8) except that the source of freshwater for diminishing convection in regions of active background convection in REF versus NID or DFC is now provided by ice advection into these regions rather than by the freshwater release effect itself.

The final set of experiments (Fig. 9) shows a substantial increase in SH overturning (about 5 Sv) with an increase of the turbulent heat fluxes over ice, either by a given factor (ETH versus REF: Fig. 9, bottom, versus Fig. 1) or by employing daily instead of monthly winds (DWF versus DWF.DFO: Fig. 9, top, versus Fig. 9, middle). In the DWF.DFO case the impact on the SH cell is minor (DWF.DFO versus REF). With respect to the SH cells these results are consistent with the strength of total SH convection (Fig. 5d). The strength of the SO cell experiences a reduction in all three experiments with the penetration depth remaining unchanged in comparison to REF. The reason for this is associated with the opposite tendency of what has been shown for the SSI, NID, and DFC cases, namely a reduction in high-latitude convection and an increase in lower-latitude convection. This seems to be due to a relatively higher variability closer to the lower-latitude westerlies, which become sites of more enhanced ice formation in wintertime (Fig. 10). The overall increase in convection being weak while the SH cell is substantially enhanced suggests that the blend of water masses produced through lower- and higher-latitude convection (product water) is associated with an increase in density (see next section).

First, changes in the global-mean potential temperature ( $\Theta$ ) and salinity ( $S$ ) at 4000-m depth will be investigated (Table 1). Overall, Table 1 reveals that  $\Theta$  and  $S$  are underestimated in the reference simulation versus the observed climatology of Levitus (1982). This seems to be widespread in global OGCM simulations (e.g., Duffy and Caldeira 1997).

Assuming that our model produces AABW by open ocean convection only, we would expect an increase (decrease) in  $\Theta$  and  $S$  of bottom water with a decrease (increase) in SO sea ice formation, the latter being associated with a decrease (increase) in SH convection followed by a decrease (increase) in the rate of AABW formation. The associated first-order mechanism is thus a cooling and freshening of CDW. Excluding NTP, NID, DFC, and DWF.DFO as yielding minor changes only, we indeed register an increase in  $\Theta$  and  $S$  at 4000 m for those experiments that yield reduced SH convection (Fig. 5), that is, SSI and SNC, and a cooling and freshening in experiments SSI.WSE (versus SSI), DWF, and ETH, which are associated with enhanced SH convection.

While the tendencies of the deep-ocean  $\Theta$  and  $S$  changes are consistent with the changes in the strength of the SH cell, there are substantial quantitative discrepancies. In the SSI experiment, for example, the strong increase in deep-ocean temperature is not accompanied by a strong reduction of the SH cell. Also, SNC reveals a stronger effect on the deep-ocean thermohaline properties than anticipated from the small changes in SH convection and the overturning cells. This seems to be related to the mixing (or entrainment) of dense water formed at the surface of the high-latitude embayments (source water) with surrounding water on the outflow path to the deep ocean, as mentioned earlier. In our model SO, such a blend of water masses (product water) will be highly dependent on the spatial convection pattern.

To elaborate this issue, the areal distribution of potential temperature and salinity at 3000-m depth for DWF (Fig. 11) and SSI (Fig. 12) are presented as differences to the reference case. Overall, these figures reflect the tendencies already noticed in Table 1. In addition, we find that the changes are almost entirely confined to the SH. Furthermore, the spatial patterns reveal regional changes of opposite sign. In the DWF case, the temperature and salinity reductions are essentially controlled by local convection features along the coast. The higher convection along East Antarctica is correlated with higher variance in the wind field.

In the SSI experiment, the regional cooling and freshening in the western Weddell Sea and off the Patagonian shelf is associated with the enhanced convection in the central Weddell Sea. Figure 13 shows the associated change in sea level, which essentially reflects density changes in the deep ocean. Comparing with Fig. 12, it is obvious that in the areas of reduced convection (along East Antarctica from 20°W to 60°E and along the coast of the eastern Ross Sea and the Amundsen Sea; see Fig. 7, top) the decrease in density is mainly due to an increase in temperature. In areas of enhanced convection, on the other hand, such as the central Weddell Sea and the western Ross Sea, the density decrease follows more a decrease in salinity in the CDW core. In the SO, the enhanced deep-ocean temperature in SSI versus REF is roughly offset by the enhanced salinity, leading to the overall weak impact on the SH cell.

In the other experiments, there is no strong counteracting mechanism like brine versus freshwater release. Enhanced convection at lower latitudes will cool (and freshen) CDW, while higher-latitude convection will mostly support this tendency. Specifically, higher-latitude convection will be associated with relatively less cooling and less freshening than lower-latitude convection, which will provide a somewhat saltier ingredient to finally form denser AABW (product water). Overall, this will lead to a cooling (and freshening) of AABW and an enhanced outflow of AABW into the world's oceans.

#### *d. Ice thickness*

In this section we examine the sensitivity of sea ice thickness to changes in the formulation of the sea ice model and its forcing. Changes in the ice thickness distribution are mainly due to the nature of sea ice to sensitively depend on changes in the ocean (and the atmosphere). As pointed out in section 3, the overall performance in terms of the spatial ice thickness pattern is moderate. The major reasons for the deficiencies are identified in the following.

The most pronounced changes in ice thickness occur in experiments SSI and SSI.WSE, while the change in DWF is small. Figure 14 (left) shows the difference of the SH winter ice-thickness pattern for SSI minus REF; the difference between SSI.WSE and REF is similar, though weaker (Fig. 14, right). Note that the interval is 0.5 m. In both cases, we mostly experience a substantial increase in ice thickness. Weak reductions are visible in the central Weddell and Ross Seas, the regions of active background convection.

Typical model wintertime temperature and salinity profiles (Fig. 15, middle) in a region of enhanced ice thickness (e.g., around 65°S, 30°E; full line; marked with "A" in Fig. 14) and in a region of slightly reduced ice thickness (e.g., around 70°S, 40°W; dashed line; marked with "B" in Fig. 14), show substantially different  $\Theta$  and  $S$  characteristics. We call region A the ice-covered region and region B a polynya region since it was mainly occupied by anomalously low ice thickness and concentration in the REF case (Fig. 4, right). While region A is characterized by a stabilizing salinity gradient and a destabilizing temperature gradient down to 2000-m depth, region B is more or less mixed. The  $\Theta$  and  $S$



maxima at the ice-covered location can be associated with CDW, whereas the water mass at the “polynya” location seems to be a product of vigorous vertical mixing down to the bottom. Compared to observed profiles at these locations (Fig. 15, top), which are based on historic hydrographic data and are biased toward summer conditions (Kim 1995), substantial discrepancies are visible. At the ice-covered location (65°S, 30°E), the  $\Theta$  and  $S$  maxima associated with CDW are fairly realistic. The vertical shape, however, reveals an excessively thick pycnocline in the REF simulation, indicating excessive vertical diffusion in the model. While the tendency of the differences seems to be captured at the polynya location, the magnitudes are far off, the main water body being too cold and too fresh. The excessive vertical mixing is more a situation expected to occur over the continental shelf, as indicated in Fig. 14 (left) by the dotted profile.

In the SSI case (Fig. 15, bottom), the temperature maximum at the ice-covered location encounters a substantial increase versus REF, together with a salinity increase below 600 m. This situation is associated with the reduced lower-latitude convection, thus enhancing the characteristics of CDW, which appears to coincide with an effective reduction in deep convection (Legutke et al. 1997). Due to the release of salty meltwater in the polynya region, the upper 1200 m have become completely mixed in the SSI case.

In summary, the tendencies of the profiles in the ice-covered region where convection is moderate compare reasonably with observed profiles, except for the excessively diffuse pycnocline and the magnitude of  $\Theta$  in the lower layers. The profiles in the polynya region, however, show a severe overestimation of vertical mixing, resembling more of what is expected over continental shelves where convection is normally not associated with direct tapping of warm deep water. In our case, however, we experience deep convection in regions where warm water masses are directly accessed. This leads regionally to a permanent underestimation of ice thickness.

## 6. Summary and conclusions

We employed a global primitive-equation OGCM that we upgraded to allow for detailed surface heat-balance calculations over partially ice-covered grid cells in addition to the existing viscous–plastic ice dynamics. For the present investigation we used a coarse-resolution model (3.5° × 3.5° × 11-layers) in order to allow for a series of near-equilibrium sensitivity experiments and climatological monthly mean forcing. Initialized from a 10 000-year spinup run, our reference simulation consists of a 1000-year near-equilibrium integration using the new sea ice thermodynamics routines. It shows a reasonable large-scale performance of the model as demonstrated by the global meridional overturning circulation, the distribution of the main water masses, the transports at various key points of the thermohaline conveyor-belt circulation, and the seasonal and spatial variations of convection. The model yields an acceptable seasonal representation of the integrated sea ice cover in both hemispheres; the spatial distributions, however, are less realistic. In the NH, sea ice is generally too thick, especially in the Beaufort Sea, which is mainly due to the coarse grid resolution; in the SH, sea ice is generally too thin, especially in the central Weddell and Ross Seas, mostly due to vigorous convection associated with excessive tapping of warm water from deeper layers. The latter has also been observed in other global OGCM studies that include the high southern latitudes.

Our sensitivity experiments focus on various possible effects of modifications in the treatment of the upper boundary conditions in the SO by imposing changes to the description and forcing of sea ice. We investigated the effect of the sea ice’s low salinity, that is, brine release during sea ice formation and freshwater release during sea ice melt as produced by the sea ice model. In this context, we also tested the effect of “salinity enhancement” as a commonly used substitute to implementing an interactive sea ice model. These two experiments revealed that both the “real” sea ice effect and its substitute lead to a substantial cooling (and freshening) of the deep ocean, while only the latter leads to a somewhat more enhanced flow of AABW into the world’s oceans (SH cell). The interactive nature of the “real” sea ice effect in our model is such that in areas of predominant freezing and brine release, mostly around the coast of East Antarctica, deep water (CDW) will be subject to a cooling and freshening. In regions of predominant melting in the model, especially in regions of intensive background convection, as occurs in the central Weddell Sea, the sea surface salinity is subject to a freshening, keeping the tongue of CDW warmer and saltier. AABW being a product of turbulent entrainment of CDW modified by lower-latitude convection and source water from the higher latitudes seems to finally lead to an overall compensation in density of AABW. Thus, the outflow of AABW into the world’s oceans (SH cell) will be rather unaffected, while AABW itself becomes cooler and fresher. If we substitute the “real” sea ice effect by salinity enhancement, the impact on the SH cell is slightly larger since the compensating melting effect in higher latitudes will be superimposed by the restoring to higher sea surface salinities.


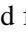

With respect to the impact on sea ice itself, brine release induces upward heat flux, which tends to melt sea ice, thus counteracting brine release. Vice versa, if brine release is neglected, ice growth is not associated with a densening of the upper layer, stabilizing the water column and leading to a significant increase in SO sea ice thickness, except for the central Weddell and Ross Seas where ice melt leads to enhanced convection and tapping of warm CDW.

Our second set of experiments addresses the role of changes in the formulation of ice thermodynamics. The inclusion of a snow cover increases the deep ocean’s temperature consistent with an overall decrease in SH convection originating from a decrease in sea ice growth. Otherwise, the impacts of these experiments are rather small. Concerning the thermodynamic forcing, however, we note that our final experiment with a specified increase of the turbulent heat flux over the SO sea ice–

ocean admixture revealed the strongest effect, the main contribution being due to the enhancement over the ice-free part of a model grid cell. These subgrid-scale openings determine the bulk of newly formed sea ice and thus contribute most to brine release. With this respect, the surface heat balance and the sea ice thermodynamics over leads constitute the most sensitive component in the southern high-latitude buoyancy forcing.

The third set of experiments was performed in order to estimate the possible effect of changes in the treatment of ice dynamics. More realistic ice dynamics seem to enhance total SH wintertime convection, while the impact on the intrusion of AABW as well as the deep-ocean  $\Theta$  and  $S$  is rather small. Caution must be expressed with regard to this statement because of the highly nonlinear interactions between the wind forcing, sea ice dynamics, and associated changes in ice thickness and ice concentration, which may alter the preconditioning for the thermodynamic processes, especially with respect to applying higher (than monthly) wind variability. Further investigations on this matter are in progress.

The final set of experiments deals with the role of the wind forcing of SO sea ice. Enhanced AABW formation, expressed by substantially lower deep-ocean temperatures and salinities, and by a significant increase of the strength of the SH overturning cell, are registered if the turbulent heat fluxes over the sea-ice–ocean admixture are calculated based on daily winds, or if they are just increased by an equivalent factor while using the monthly winds. In these cases, total SH convection is substantially higher in SH fall. If daily wind fluctuations are applied to force the ice pack only dynamically, the overall impact is small. These results suggest that the high sensitivity of SO sea ice to the way it is forced by the atmosphere does transfer to the deep-ocean water-mass characteristics and to the large-scale thermohaline circulation. This implies that different feedback mechanisms associated with the usage of interactive atmospheric boundary-layer schemes or coupled atmosphere–sea-ice–ocean GCMs to determine the (southern) high-latitude surface conditions may create sensitive influences on global-scale model-ocean properties.

The impact on the zonally integrated meridional heat transport was relatively small: maximum 10% in a zonal band around 50°S in the ETH experiment. Further changes of up to 10% occurred in the strength of the ACC (or rather Drake Passage throughflow). In cases of colder deep water (see [Table 1](#) , DWF and ETH) the ACC increased by about 5 Sv. In the cases of warmer deep water (SSI and SNC) the ACC decreased to 3.5 Sv. These changes are consistent with a general increase of the density gradient across the ACC as inferred from [Figs. 11–13](#) . It also appears from [Fig. 13](#)  that the brine-release effect in the model mainly acts to increase deep-water density along the coast between 20°W and 60°E, as well as between 170°W and 120°W. The resulting outflow patterns seem to reflect the outflow paths of the Weddell and Ross Sea (deep western boundary current) as observed for example, by [Coles et al. \(1996\)](#) in the southwest Atlantic and by [Johnson and Orsi \(1997\)](#) in the southwest Pacific.

The general conclusion is that the way sea ice is formulated and forced in a global OGCM does not only modify the regional stratification and convection rates but has also remote effects on the deep-ocean hydrographic properties as well as the penetration of AABW into the World Ocean. From the selection of our experiments, the strongest changes occurred with the brine-release effect (as well as with salinity enhancement as its crude substitute) and the effect of wind variability on sea ice thermodynamics. A further significant long-term impact on the deep water-mass characteristics was associated with the insulation effect of a snow cover on top of sea ice.

This paper leaves a series of open questions. While we discussed some regional features around Antarctica, a lot of regional aspects are still at odds and need to be improved. Specifically, since our results suggest that the decision whether there is a global impact or not depends heavily on the processes at individual convective sites, the realism of their regional representation may become decisive. As an example, we cannot assure that the weak impact of the spatially variable brine- and freshwater-release effects on the SH cell is real (especially since others found a stronger impact) or just due to the high background convection in the high-latitude embayments.

The observational evidence suggests that the main source of brine eventually influencing bottom-water formation is provided by new-ice growth over the continental shelves (e.g., [Martinson 1990](#); [Gordon and Huber 1990](#); [England 1992](#); [McPhee 1995](#); [Killworth 1979](#)). It has generally been recognized that a mixture of cold and saline shelf water with the warm and saline remnant of NADW, called Lower CDW (LCDW), will ultimately constitute the ingredient producing AABW ([Jacobs et al. 1985](#); [Toggweiler and Samuels 1995](#); [Kim 1995](#); [Killworth 1983](#); [Foster and Carmack 1976](#); [Gill 1973](#)). Special emphasis thus needs to be given to the impact of brine release on convection and to a proper weight between open ocean and near-boundary convection in the present type of ocean climate model.

In preliminary experiments we found that one way to reduce open ocean convection in favor of near-boundary convection is to widen the continental shelves to provide an appropriate brine reservoir. Concerning the impact of brine release on convection, [Legutke et al. \(1997\)](#) and [Duffy and Caldeira \(1997\)](#) indicated an improvement by distributing released brine from sea ice formation immediately over two or more subsurface model layers. Together with dumping melt water in the upper layer only, this has the effect of enhancing the vertical stratification, accompanied by reduced deep convection, and virtually allowing LCDW to more closely approach the continental slope. The application of ocean mixed layer physics in conjunction with comprehensive sea ice physics in this region ([McPhee 1995](#); [Lemke et al. 1990](#)) may lead to a more promising and justifiable approach. The deficiencies in the present model's SH sea ice characteristics are mainly a result of

these convection issues.

Finally, a higher model resolution around Antarctica is naturally expected to improve the regional hydrography in this ocean climate model. We have to keep in mind, though, that we aim at a series of near-equilibrium experiments to figure the sensitivity related to the high-latitude surface conditions. This imposes limits on computational demands.

We stress that this study is more an introduction to a complex field of linking regional-scale processes to global-scale ocean climate features. The highly nonlinear and interactive character of sea ice modifying the surface conditions together with the direct link between surface and deep-water conditions gives the polar oceans a peculiar and yet decisive role in the global climate system. This topic provides a forum for a series of further investigations and refinements to gradually filter out those high-latitude processes that influence the large-scale properties in an ocean climate model most crucially.

### Acknowledgments

This paper benefited from discussions with various colleagues, especially Hugues Goosse, Stephanie Legutke, Ernst Maier-Reimer, Uwe Mikolajewicz, Alejandro Orsi, and Tom Whitworth. We are thankful for the various constructive comments of two anonymous reviewers. This research was primarily supported by the College of Geosciences at Texas A&M University (TAMU), who also provided a DEC alpha workstation, which was used to perform about 50% of the experimental computations. The other 50% were conducted on the Cray J90 of the TAMU Supercomputing Facility. The 10 000-year spinup run was conducted on the Cray-YMP of the German Climate Computing Center (DKRZ) at Hamburg.

---

### REFERENCES

- Akitomo, K., T. Awaji, and N. Imasato, 1995: Open-ocean deep convection in the Weddell Sea: Two-dimensional numerical experiments with a nonhydrostatic model. *Deep-Sea Res.*, **42**(1), 53–73..
- Bryan, K., 1969: Climate and the ocean circulation, III. The ocean model. *Mon. Wea. Rev.*, **97**, 806–827.. [Find this article online](#)
- Cai, W., and P. G. Baines, 1996: Interactions between thermohaline- and wind-driven circulations and their relevance to the dynamics of the Antarctic Circumpolar Current, in a coarse-resolution global ocean general circulation model. *J. Geophys. Res.*, **101**(C6), 14 073–14 093..
- Carmack, E. C., 1990: Large-scale physical oceanography of polar oceans. *Polar Oceanography, Part A: Physical Science*, W. O. Smith, Ed., Academic Press, 171–222..
- Coles, V. J., M. S. McCartney, D. B. Olson, and W. M. Smethie, 1996: Changes in Antarctic bottom water properties in the western South Atlantic in the late 1980s. *J. Geophys. Res.*, **101**(C4), 8957–8970..
- Cox, M. D., 1984: A primitive equation, 3-dimensional model of the ocean, GFDL Ocean Group Tech. Rep. No. 1, GFDL/Princeton University, 141 pp..
- Cubasch, U., K. Hasselmann, H. Höck, E. Maier-Reimer, U. Mikolajewicz, B. D. Santer, and R. Sausen, 1992: Time-dependent greenhouse warming computations with a coupled ocean–atmosphere model. *Climate Dyn.*, **8**, 55–69..
- , U., Santer, B. D., Hellbach, A., Hegerl, G., Höck, H., Maier-Reimer, E., Mikolajewicz, U., Stössel, A., Voss, R. 1994: Monte Carlo climate change forecasts with a global coupled ocean–atmosphere model. *Climate Dyn.*, **10**, 1–19..
- Danabasoglu, G., J. C. McWilliams, and W. G. Large, 1996: Approach to equilibrium in accelerated global oceanic models. *J. Climate*, **9**, 1092–1110.. [Find this article online](#)
- Drijfhout, S. S., C. Heinze, M. Latif, and E. Maier-Reimer, 1996: Mean circulation and internal variability in an ocean primitive equation model. *J. Phys. Oceanogr.*, **26**, 559–580..
- Duffy, P. B., and K. Caldeira, 1997: Sensitivity of simulated salinity in a three-dimensional ocean model to upper ocean transport of salt from sea-ice formation. *Geophys. Res. Lett.*, **24**(11), 1323–1326..
- England, M. H., 1992: On the formation of Antarctic intermediate and bottom water in ocean general circulation models. *J. Phys. Oceanogr.*, **22**, 918–926..
- , 1993: Representing the global-scale water masses in ocean general circulation models. *J. Phys. Oceanogr.*, **23**, 1523–1552..
- Foster, T. D., and E. C. Carmack, 1976: Frontal zone mixing and Antarctic bottom-water formation in the southern Weddell Sea. *Deep-Sea*

Gill, A. E., 1973: Circulation and bottom-water production in the Weddell Sea. *Deep-Sea Res.*, **20**, 111–140..

Goosse, H., J. M. Campin, T. Fichefet, and E. Deleersnijder, 1997: The impact of sea-ice formation on the properties of Antarctic bottom water. *Ann. Glaciol.*, **25**, 276–281..

Gordon, A. L., 1978: Deep Antarctic convection west of Maud Rise. *J. Phys. Oceanogr.*, **8**, 357–377..

—, and B. A. Huber, 1990: Southern Ocean winter mixed layer. *J. Geophys. Res.*, **95**, 11 655–11 672..

Gordon, H. B., and S. P. O'Farrell, 1997: Transient climate change in the CSIRO coupled model with dynamic sea ice. *Mon. Wea. Rev.*, **125**, 875–907.. [Find this article online](#)

Häkkinen, S., 1995: Simulated interannual variability of the Greenland Sea deep-water formation and its connection to surface forcing. *J. Geophys. Res.* **100**(C3), 4761–4770..

Hasselmann, K., 1982: An ocean model for climate variability studies. *Progress in Oceanography*, Vol. 11 Pergamon, 69–92..

Hellerman, S., and M. Rosenstein, 1983: Normal monthly wind stress over the world ocean with error estimates. *J. Phys. Oceanogr.*, **13**, 1093–1104..

Hibler, W. D., III, 1979: A dynamic thermodynamic sea ice model. *J. Phys. Oceanogr.*, **9**, 815–846..

—, and K. Bryan, 1987: A diagnostic ice–ocean model. *J. Phys. Oceanogr.*, **17**, 987–1015..

—, and J. E. Walsh, 1982: On modeling seasonal and interannual fluctuations of Arctic sea ice. *J. Phys. Oceanogr.*, **12**, 1514–1523..

Jacobs, S. S., and J. C. Comiso, 1989: Sea ice and oceanic processes on the Ross Sea continental shelf. *J. Geophys. Res.*, **94**, 18 195–18 211..

—, R. G. Fairbanks, and Y. Horibe, 1985: Origin and evolution of water masses near the Antarctic continental margin: Evidence from H2180/H2160 ratios in sea water. *Oceanology of the Antarctic Continental Shelf*. S. S. Jacobs, Ed., Antarctic Research Series **43**, 59–85..

Johnson, G. C., and A. H. Orsi, 1997: Southwest Pacific ocean water-mass changes between 1968/69 and 1990/91. *J. Climate*, **10**, 306–316.. [Find this article online](#)

Killworth, P. D., 1979: On “chimney” formations in the ocean. *J. Phys. Oceanogr.*, **9**, 531–554..

—, 1983. Deep convection in the world ocean. *Rev. Geophys. Space Phys.*, **21**(1), 1–26..

Kim, S.-J., 1995: The transition zone between the oceanic and shelf regimes around Antarctica. M.S. thesis, Dept. of Oceanography, Texas A&M University, 70 pp..

Latif, M., T. Stockdale, J.-O. Wolff, G. Burgers, E. Maier-Reimer, M. M. Junge, K. Arpe, and L. Bengtsson, 1994: Climatology and variability in the ECHO coupled GCM. *Tellus*, **46A**, 351–366..

Legutke, S., 1992: A simulation of the Arctic sea ice cover. Rep. No. 30, Alfred-Wegener-Institut fuer Polar- und Meeresforschung, Bremerhaven, Germany..

—, E. Maier-Reimer, A. Stössel, and A. Hellbach, 1997: Ocean sea ice coupling in a global general ocean circulation model. *Ann. Glaciol.*, **25**, 116–120..

Lemke, P., W. B. Owens, and W. D. Hibler III, 1990: A coupled sea-ice–mixed-layer–pycnocline model for the Weddell Sea. *J. Geophys. Res.*, **95**(C6), 9513–9525..

Levitus, S., 1982. *Climatological Atlas of the World Ocean*. NOAA Prof. Paper No. 13, U.S. Govt. Printing Office, 173 pp..

MacDonald, A. M., and C. Wunsch, 1996: An estimate of global ocean circulation and heat fluxes. *Nature*, **382**, 436–439..

Maier-Reimer, E., 1993: The driving force of brine rejection on the deepwater formation in the Hamburg LSG OGCM. *Ice in the Climate System*, W. R. Peltier, Ed., Springer-Verlag, NATO-ASI Series, Vol. I 12, 211–216..

—, U. Mikolajewicz, and K. Hasselmann, 1993. Mean circulation of the Hamburg LSG OGCM and its sensitivity to the thermohaline surface forcing. *J. Phys. Oceanogr.*, **23**, 731–757..



Manabe, S., M. J. Spelman, and R. J. Stouffer, 1992: Transient responses of a coupled ocean–atmosphere model to gradual changes of atmospheric CO<sub>2</sub>. Part II: Seasonal response. *J. Climate*, **5**, 105–126.. [Find this article online](#)

Martinson, D. G., 1990: Evolution of the Southern Ocean winter mixed layer and sea ice: Open ocean deep water formation and ventilation. *J. Geophys. Res.*, **95**, 11 641–11 654..

— ↵1993: Ocean heat and sea ice thickness in the Southern Ocean. *Ice in the Climate System*, W. R. Peltier, Ed., Springer-Verlag, NATO-ASI Series, Vol. I 12, 597–609..

— ↵P. D. Killworth, and A. L. Gordon, 1981: A convective model for the Weddell Polynya. *J. Phys. Oceanogr.*, **11**, 466–488..

McPhee, M. G., 1995: Turbulent oceanic heat flux during winter in the central Weddell Sea. *Fourth Conf. on Polar Meteorology and Oceanography*, Dallas, TX, Amer. Meteor. Soc., 214–217..

Meehl, G. A. and W. M. Washington, 1990: CO<sub>2</sub> climate sensitivity and snow-sea-ice albedo parameterization in an atmospheric GCM coupled to a mixed-layer ocean model. *Climate Change*, **6**, 283–306..

Mikolajewicz, U., and E. Maier-Reimer, 1990; Internal secular variability in an ocean general circulation model. *Climate Dyn.*, **4**, 145–156..

Murphy, J. M., 1995: Transient response of the Hadley Centre coupled ocean–atmosphere model to increasing carbon dioxide. Part I: Control climate and flux adjustment. *J. Climate*, **8**, 36–56.. [Find this article online](#)

— ↵and J. F. B. Mitchell, 1995: Transient response of the Hadley Centre coupled ocean–atmosphere model to increasing carbon dioxide. Part II: Spatial and temporal structure of response. *J. Climate*, **8**, 57–80.. [Find this article online](#)

Oshima, K. I., T. Takizawa, S. Ushio, and T. Kawamura, 1996: Seasonal variations of the Antarctic coastal ocean in the vicinity of Lützow-Holm Bay. *J. Geophys. Res.*, **101**(C9), 20 617–20 628..

Owens, W. B., and P. Lemke, 1990: Sensitivity studies with a sea ice–mixed layer–pycnocline model in the Weddell Sea. *J. Geophys. Res.*, **95**, 9527–9538..

Pacanowski, R. C., 1995: MOM 2 Documentation user’s guide and reference manual. Version 1. GFDL Ocean Tech. Rep. No. 3. GFDL, Princeton, NJ, 232 pp..

Price, J. F., and M. O’N. Baringer, 1994: Outflows and deep water production by marginal seas. *Progress in Oceanography* Vol. 33, Pergamon Press, 161–200..

Schlosser, P., R. Bayer, A. Foldvik, T. Gammelsrød, G. Rohardt, and K. O. Munnich, 1990: Oxygen 18 and helium as tracers of ice shelf water and water/ice interaction in the Weddell Sea. *J. Geophys. Res.*, **95**, 3253–3263..

Schmitz, W. J., Jr., 1996: On the world ocean circulation: Vol. I. Tech. Rep. WHOI-96-03, Woods Hole, MA, 141 pp..

Semtner, A. J., 1976: Numerical simulation of the Arctic Ocean circulation. *J. Phys. Oceanogr.*, **6**, 409–425..

Stössel, A., 1996: On the ocean’s upper boundary conditions in regions influenced by sea ice. *Physica D*, **98**, 614–624..

— ↵1997: On the impact of sea ice in a global ocean circulation model. *Ann. Glaciol.*, **25**, 111–115..

— ↵and W. B. Owens, 1992: The Hamburg sea-ice model. Tech. Rep. 3. Deutsches KlimaRechenZentrum, Hamburg, Germany, 61 pp..

— ↵P. Lemke, and W. B. Owens, 1990: Coupled sea ice–mixed layer simulations for the Southern Ocean. *J. Geophys. Res.*, **95**, 9539–9555..

— ↵J. M. Oberhuber, and E. Maier-Reimer, 1996: On the representation of sea ice in global ocean general circulation models. *J. Geophys. Res.*, **101**(C8), 18 193–18 212..

Toggweiler, J. R., and B. Samuels, 1995: Effect of sea ice on the salinity of Antarctic bottom waters. *J. Phys. Oceanogr.*, **25**, 1980–1997..

Washington, W. M., and G. A. Meehl, 1996: High-latitude climate change in a global ocean–atmosphere–sea ice model with increased atmospheric CO<sub>2</sub>. *J. Geophys. Res.*, **101** (D8), 12 797–12 801..

Weatherly, J. W., T. W. Bettge, and W. M. Washington, 1997: Simulation of sea ice in the NCAR Climate System Model. *Ann. Glaciol.*, **25**, 107–110..

Whitworth, T. III, and R. G. Peterson, 1985: Volume transport of the Antarctic circumpolar current from bottom pressure measurements. *J. Phys. Oceanogr.*, **15**, 810–816..

Wolff, J.-O., E. Maier-Reimer, and S. Legutke, 1997: The Hamburg Ocean Primitive Equation model HOPE. Tech. Rep. 13. Deutsches Klimarechenzentrum, Hamburg, Germany, 98 pp..

Woodruff, S. D., R. J. Slutz, R. L. Jenne, and Streurer, 1987: A Comprehensive Ocean–Atmosphere Data Set. *Bull. Amer. Meteor. P. Soc.*, **68**, 1239–1250..

Worby, A. P., N. L. Bindoff, V. I. Lytle, I. Allison, and R. A. Massom, 1996: Winter ocean/sea ice interactions studied in the east Antarctic. *Eos*, **77**(46), 453–457..

Wu, X., I. Simmonds, and W. F. Budd, 1996: Comparison of sea ice simulations with interactive and monthly averaged forcing models. *J. Geophys. Res.*, **101** (D5), 9359–9374..

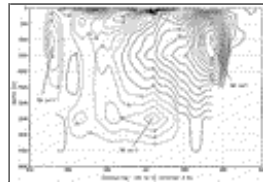
## Tables

Table 1. List of experiments, including global and annual mean potential temperature and salinity at 4000 m, and integration time.

Experiment abbreviation	Experiment description	$\bar{\theta}$ (°C)	$\bar{S}$ (psu)	Integration time (yr)
OBS	Observation (Levitus 1982)	0.70	34.740	—
REF	Reference experiment	0.45	34.687	1000
SI	Stably stratified sea ice	0.82	34.653	1000
SSIWBE	Stably stratified sea ice plus wintertime salinity enhancement	0.44	34.632	300
NTP	No sea-ice thickness growth in ice-free part of a grid cell	0.49	34.636	600
SN	Snow cover	0.62	34.647	600
ND	No ice dynamics	0.44	34.633	300
DC	Dynamic forcing only via ocean currents	0.45	34.637	300
DWF	Daily wind fluctuation (monthly mean plus daily wind fluctuation)	0.36	34.629	300
DWCFD	Daily wind fluctuation for dynamic forcing only	0.47	34.637	300
ETH	Enhanced turbulent heat flux	0.60	34.625	1000

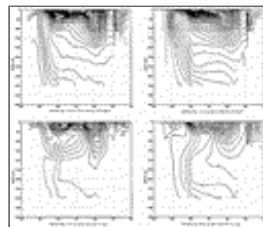
[Click on thumbnail for full-sized image.](#)

## Figures



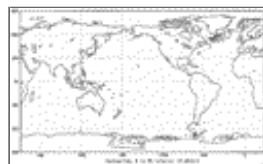
[Click on thumbnail for full-sized image.](#)

Fig. 1. Annual-mean global meridional overturning circulation of the reference experiment (REF).



[Click on thumbnail for full-sized image.](#)

Fig. 2. Annual-mean meridional section of western Atlantic (averaged between 60° and 10°W) potential temperature (top) and salinity (bottom) as observed according to [Levitus \(1982\)](#) (left) and as simulated in REF (right).



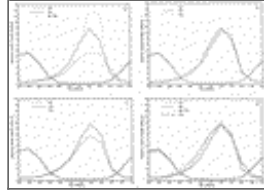
[Click on thumbnail for full-sized image.](#)

Fig. 3. Annual-mean potential energy release associated with convection as simulated in REF.



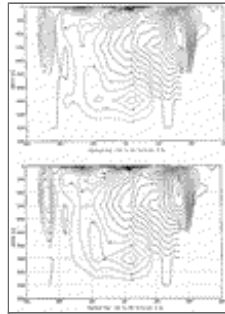
[Click on thumbnail for full-sized image.](#)

Fig. 4. Winter ice thickness distribution in the Northern Hemisphere (left) and the Southern Hemisphere (right) as simulated in REF.



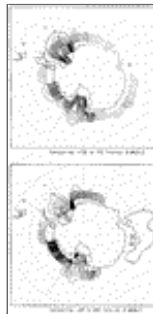
[Click on thumbnail for full-sized image.](#)

Fig. 5. Seasonal cycle of hemispherically averaged potential energy release due to convection of experiments SSI and SSI.WSE (a), NTP and SNC (b), NID and DFC (c), and DWF, DWF.DFO, and ETH (d). The REF case is displayed by a solid line in each figure.



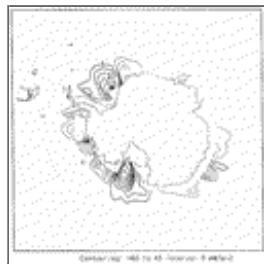
[Click on thumbnail for full-sized image.](#)

Fig. 6. Annual-mean global meridional overturning for experiments SSI (top) and SSI.WSE (bottom).



[Click on thumbnail for full-sized image.](#)

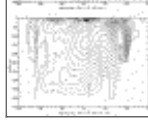
Fig. 7. Difference in SH winter (Jul, Aug, Sep) potential energy release due to convection; experiments SSI minus REF (top) and SSI.WSE minus SSI (bottom).



[Click on thumbnail for full-sized image.](#)

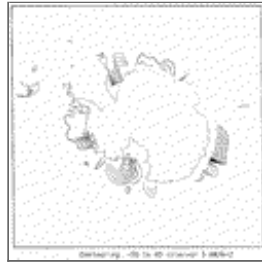
Fig. 8. Experiment NID minus REF, otherwise as [Fig. 7](#) .





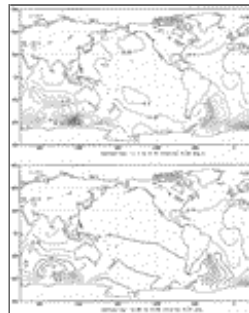
[Click on thumbnail for full-sized image.](#)

Fig. 9. Annual-mean global meridional overturning of experiments DWF (top), DWF.DFO (middle), and ETH (bottom).



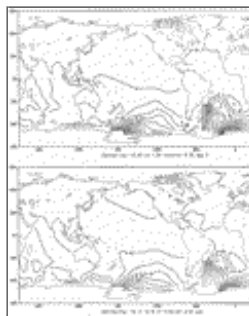
[Click on thumbnail for full-sized image.](#)

Fig. 10. Experiment DWF minus REF, otherwise as [Fig. 7](#).



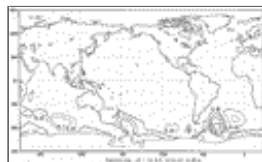
[Click on thumbnail for full-sized image.](#)

Fig. 11. Difference in annual-mean potential temperature (top) and salinity (bottom) at 3000-m depth for experiments DWF minus REF.



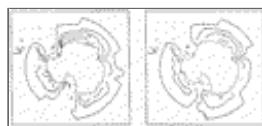
[Click on thumbnail for full-sized image.](#)

Fig. 12. Experiment SSI minus REF, otherwise as [Fig. 11](#).



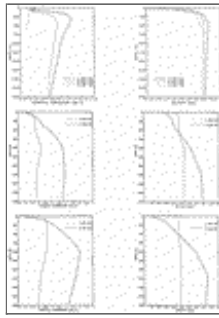
[Click on thumbnail for full-sized image.](#)

Fig. 13. Difference in annual-mean sea level elevation; experiments SSI minus REF.



[Click on thumbnail for full-sized image.](#)





[Click on thumbnail for full-sized image.](#)

Fig. 15. Vertical profiles of SH winter potential temperature (left) and salinity (right) at two selected positions in the Southern Ocean, the locations of which are marked in [Fig. 14](#); observed (see text) (top) as well as from experiments REF (middle) and SSI (bottom).

*Corresponding author address:* Dr. Achim Stössel, Department of Oceanography/TCCS, Texas A&M University, College Station, TX 77843-3146.

E-mail: [achim@advect.tamu.edu](mailto:achim@advect.tamu.edu)

[top](#) ▲



© 2008 American Meteorological Society [Privacy Policy and Disclaimer](#)  
Headquarters: 45 Beacon Street Boston, MA 02108-3693  
DC Office: 1120 G Street, NW, Suite 800 Washington DC, 20005-3826  
[amsinfo@ametsoc.org](mailto:amsinfo@ametsoc.org) Phone: 617-227-2425 Fax: 617-742-8718  
[Allen Press, Inc.](#) assists in the online publication of AMS journals.